Neutron-scattering studies of magnetism in multiferroic HoMnO$_3$ (invited)

O. P. Vajk[a)]
NIST Center for Neutron Research, Gaithersburg, Maryland 20899

M. Kenzelmann
Laboratory for Solid State Physics, ETH Hönggerberg, CH-8093 Zürich, Switzerland
and Laboratory for Neutron Scattering, ETHZ and Paul Scherrer Institute, CH-5232 Villigen, Switzerland

J. W. Lynn
NIST Center for Neutron Research, Gaithersburg, Maryland 20899

S. B. Kim and S.-W. Cheong
Department of Physics and Astronomy, Rutgers University, Piscataway, New Jersey 08854

Hexagonal HoMnO$_3$ is a frustrated antiferromagnet (T_N=72 K) ferroelectric (T_C=875 K) with a rich magnetic phase diagram consisting of multiple temperature- and field-dependent phases. Previously observed anomalies in the dielectric constant at magnetic phase transitions indicate strong coupling between the ferroelectricity and magnetism. Neutron-diffraction measurements in a magnetic field reveal new intermediate-field phases at low temperatures. Inelastic neutron-scattering measurements are used to establish the primary magnetic interactions and demonstrate that the spin dynamics in HoMnO$_3$ are well described by a simple two-dimensional nearest-neighbor Heisenberg antiferromagnetic exchange J=2.44 meV and a temperature-dependent anisotropy D. © 2006 American Institute of Physics. [DOI: 10.1063/1.2162090]

I. INTRODUCTION

The technological possibilities for materials in which the electric polarization can be switched with a magnetic field[1,2] or the magnetic polarization with an electric field[3] have increased interest in studying materials with both magnetic and ferroelectric orders. Such materials, known as multiferroics, are very rare,[4] and only a select few exhibit strong coupling between the magnetic and ferroelectric orders. Theoretical understanding of such coupling is still lacking, and so finding experimental clues about the interaction of these two order parameters remains a priority.

The hexagonal rare-earth maganese oxides (RMnO$_3$, with R=Ho, Er, Tm, Yb, Lu, and Y) are a family of multiferroic materials which have attracted considerable attention in recent years. These materials order ferroelectrically well above room temperature (with $T_{FE} \approx 1000$ K) and antiferromagnetically well below room temperature ($T_N \approx 100$ K). Mn^{3+} ions (surrounded by O^{2-} ions) form two-dimensional (2D) triangular lattices of spin-2 moments in the *a-b* plane, which are then stacked in alternating fashion along the *c* axis with R^{3+} layers in between. The structure of these materials was reported in 1963,[5] followed shortly by the determination of the 120° frustrated antiferromagnetic structure of the Mn^{3+} moments.[6] Only recently, however, has there been significant interest in the interaction of the ferroelectric and magnetic order parameters in these materials. The indication of such a coupling was discovered in dielectric constant anomalies at the magnetic ordering temperature in YMnO$_3$,[7] a material already being considered as a ferroelectric storage medium.[8] Much more dramatic anomalies in the dielectric constant have been subsequently observed in HoMnO$_3$.[9,10]

The magnetic structure of HoMnO$_3$ has been studied previously with neutron powder diffraction,[6,11,12] optical second-harmonic generation (SHG),[13–16] and magnetic and dielectric susceptibles.[17] Below the magnetic ordering temperature $T_N \approx 72$ K, HoMnO$_3$ orders in a noncollinear 120° spin structure (magnetic symmetry group $P6_3'c'm$). At the spin reorientation temperature $T_{SR} \approx 40$ K, the Mn moments rotate in the plane, changing the magnetic symmetry to $P6_3'cm'$. At very low temperatures ($T_{Ho} \approx 8$ K), half the Ho moments order antiferromagnetically with moments aligned along the *c* axis, accompanied by a second spin reorientation transition of the Mn moments into the $P6_3cm$ phase. The spin structure for each of these phases is shown in Fig. 1. These transitions are accompanied by anomalies in the dielectric constant ϵ,[9,10] with a particularly sharp increase in ϵ at T_{SR}, indicating strong (though possibly indirect) coupling
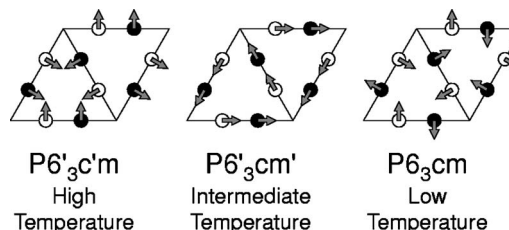
FIG. 1. The three zero-field Mn^{3+} spin configurations in HoMnO$_3$. The open circles indicate Mn ions at z=0, filled circles indicate Mn ions at z=c/2, and arrows indicate the direction of the local S=2 magnetic moments. HoMnO$_3$ initially orders in the high-temperature phase around 72 K and undergoes a spin reorientation transition to the intermediate phase at around 40 K. Below around 8 K, Ho^{3+} moments (not shown) also order, and the Mn^{3+} moments udergo a second reorientation transition into the low-temperature phase.

a)Electronic mail: owen.vajk@nist.gov
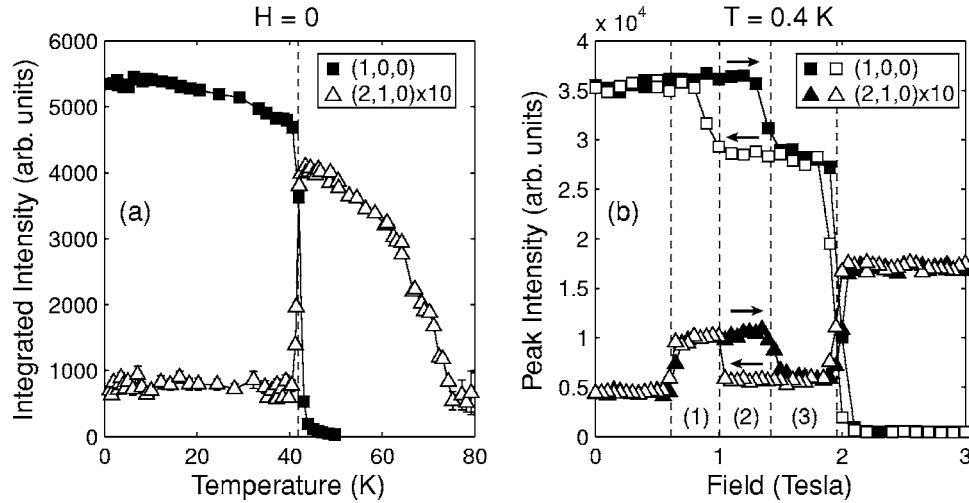
FIG. 2. Neutron-diffraction measurements of the (1,0,0) and (2,1,0) magnetic Bragg reflections. (a) Zero-field measurements show a sharp first-order spin reorientation transition between the high-temperature phase [with scattering at the (2,1,0) reflection] and the intermediate temperature phase [with scattering at the (1,0,0) reflection]. These reflections are not sensitive to the 8 K Ho ordering transition. (b) Low-temperature measurements as a function of magnetic field H applied along the c axis. The filled symbols indicate data taken with increasing field, open symbols indicate decreasing field. Intermediate phases are labeled (1) and (3), with hysteretic overlap in region (2).

between the ferroelectric and magnetic orders in $HoMnO_3$. This spin reorientation transition can be pushed to lower temperatures by the application of a magnetic field,[9,15] with T_{SR} decreasing linearly with H^2.[18] Optical measurements also indicate that the application of an electric field can not only change the symmetry of the Mn lattice, but can also induce ferromagnetic order on the Ho lattice.[3] These results suggest that $HoMnO_3$ is an ideal candidate for investigating the interaction between magnetic and ferroelectric orders in multiferroics. In order to better understand this interaction, however, a more complete picture of the magnetic properties of $HoMnO_3$ is needed. This paper describes the investigation of the magnetic phase diagram and the spin dynamics of $HoMnO_3$ using neutron-scattering studies of single crystals, and provides more details on previously reported results.[19]

II. EXPERIMENT

The zero-field magnetic phase diagram of $HoMnO_3$ is well known from both powder neutron diffraction[6,11,12] and SHG nonlinear optical measurements,[13–16] and the spin structures of the ordered phases are shown in Fig. 1. The magnetic phase diagram in a magnetic field parallel to c (the ferroelectric polarization axis) shows complicated behavior, but has previously only been observed with optical SHG measurement[15] or indirectly by observing quantities (such as the dielectric constant or heat capacity) which show anomalies at the phase boundaries.[9,10,20] Neutron-scattering measurements of the field-dependent phase diagram were still lacking. Furthermore, while the zero-field magnetic structure is well established, the strength of the actual magnetic interactions was previously unknown. In order to address these issues, single crystals of $HoMnO_3$ were grown using a traveling-solvent optical floating zone technique. Diffraction measurements of these single-crystal samples in a magnetic field were used to establish a phase diagram for $HoMnO_3$,

and the primary magnetic interactions were obtained from inelastic scattering measurements of the spin-wave dynamics.

A. Elastic neutron scattering

To investigate the magnetic-field-dependent phase diagram, a 0.5 g sample was mounted inside a vertical-field 7 T superconducting magnet with a helium-3 insert. Because the magnetic symmetry of $HoMnO_3$ changes at the spin reorientation transitions, the magnetic Bragg scattering observable with neutrons will also change. The transition from the high-temperature to the intermediate-temperature phase is typically observed by measuring the (1,0,1) reflection, which is strong in the high-temperature phase but not in the intermediate temperature phase, and the (1,0,0) reflection, which is strong in the intermediate-temperature phase but is forbidden in the high-temperature phase. In order to apply a field along the c axis in a vertical-field magnet, scattering was restricted to the $(H,K,0)$ scattering plane, preventing measurement of the (1,0,1) reflection. The (2,1,0) reflection, though approximately an order of magnitude weaker than the (1,0,1), shows the same temperature dependence in the high-temperature and intermediate-temperature phases. Figure 2(a) shows the zero-field measurements of the integrated intensity of the (1,0,0) and (2,1,0) reflections, showing both the onset of magnetic ordering at $T_N = 74$ K and the spin reorientation transition at $T_{SR} = 42$ K. These results are in good agreement with previous powder results for the (1,0,0) and (1,0,1) reflections.[6,11,12] Unfortunately, unlike the (1,0,1) reflection, the (2,1,0) reflection is not sensitive to the low-temperature phase, and so this transition was not observable in our magnetic-field measurements.

Measurements of the (1,0,0) and (2,1,0) peak intensities in an applied field $H\|c$ show that T_{SR} decreases with increasing H as previously reported.[9,15] At high fields, the transition between the intermediate- and high-temperature phases broadens, with a continuous decrease and increase in the
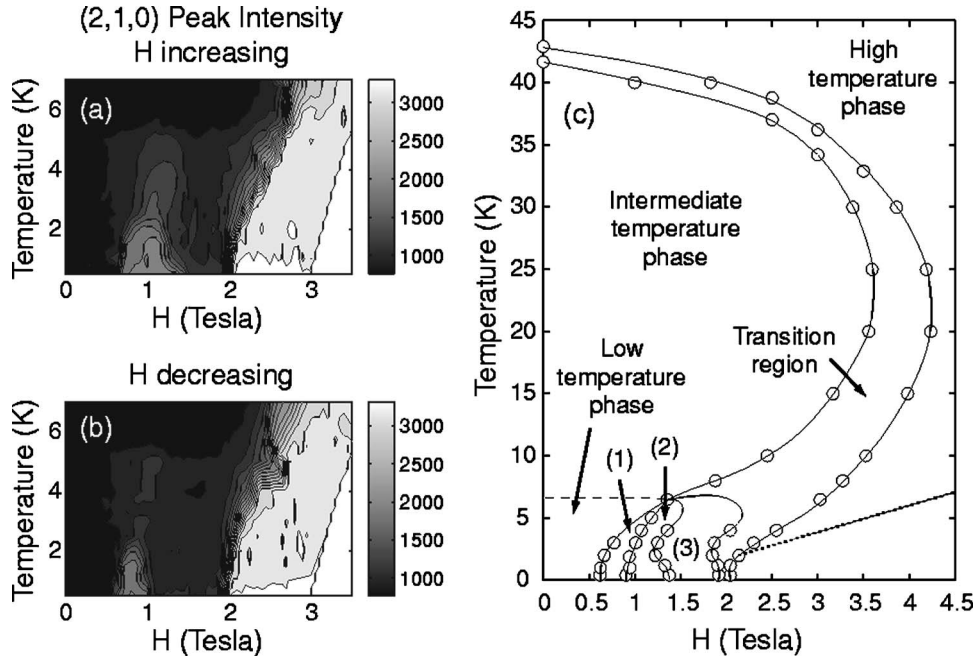
FIG. 3. Contour maps of the $(2,1,0)$ peak intensity as a function of temperature and magnetic field for (a) increasing and (b) decreasing magnetic fields. At low temperatures, the transitions are sharp, but blur together at higher temperatures. (c) Phase diagram for $HoMnO_3$ as a function of temperature and magnetic field obtained from $(1,0,0)$ and $(2,1,0)$ diffraction data. The lines are guides to the eye. The dashed line and dotted lines indicate approximate phase boundaries for previously reported transitions not observable from the $(1,0,0)$ and $(2,1,0)$ diffraction data. The numbered regions correspond to the intermediate phases and hysteretic overlap region shown in Fig. 2.

scattering intensity for the $(1,0,0)$ and $(2,1,0)$ reflections, respectively, across the transition region. At low temperatures, the transition becomes significantly more complex. Figure 2(b) shows the field dependence of the $(1,0,0)$ and $(2,1,0)$ peak intensities at 0.4 K for increasing and decreasing fields. Instead of one broad transition, there are three distinct and very sharp first-order transitions, indicating two intermediate phases [labeled (1) and (3)] as functions of magnetic field. Furthermore, the middle transition shows a very large hysteresis, with the overlap region [labeled (2)] spanning a range in field comparable to the intermediate phases themselves.

Figures 3(a) and 3(b) show contour maps of the $(2,1,0)$ peak intensity (with H increasing and decreasing, respectively) as a function of H and T. As temperature increases, these intermediate transitions broaden and fade, until only a single, broad transition is observable at higher temperatures. The phase diagram obtained from these measurements is shown in Fig. 3(c), along with phase boundaries previously reported[15] but not observable from the $(1,0,0)$ and $(2,1,0)$ data.

B. Inelastic neutron scattering

Inelastic neutron-scattering measurements of the spin-wave dispersion and crystal-field levels were performed on a 1.8 g single crystal on the BT-2 and BT-9 thermal triple-axis spectrometers and the cold-neutron spin-polarized triple-axis spectrometer (SPINS) at the NIST Center for Neutron Research. Two crystal-field levels were previously reported at 1.5 and 3.1 meV,[19] which complicated the measurements of the low-energy spin-wave dispersion. To investigate these crystal-field levels in more detail, high-energy-resolution scans were performed on SPINS. Figure 4 shows an energy scan taken with a focusing analyzer at $\mathbf{Q}=(1.2,0,0)$ and $T=20$ K. In addition to the two previously reported crystal-field levels at 1.48(2) and 3.13(2) meV, a third intermediate crystal-field level was also observed at 2.41(3) meV, though its intensity is much weaker. Measurements at different mo-

mentum transfers show that all three excitations are dispersionless. Polarized beam measurements performed on BT2 show that the 1.48 and 3.13 meV modes are indeed magnetic (confirming that these are crystal-field excitations), though the 2.41 meV mode could not be resolved in those measurements.

Measurements of the spin-wave dispersion were performed on BT-2 and BT-9. Figure 5 shows typical constant-$\mathbf{Q}$ inelastic scans taken at 20 K on BT2 with 60′-40′-40′-80′ collimations. Figure 5(a) shows scans at two different H positions with 14.7 meV fixed final energy, revealing two magnon branches dispersing in the plane. Figure 5(b) shows scans at different L positions taken with 14.7 meV fixed incident energy, and show no dispersion in the out-of-plane direction within the uncertainties. The clear in-plane dispersion and lack of out-of-plane dispersion indicate that the spin dynamics in $HoMnO_3$ are primarily 2D. Inelastic scans were performed at a variety of $\mathbf{Q}$ positions in the plane along the high-symmetry directions of the reciprocal lattice, as shown by the arrows in the schematic of Fig. 6(a). The peak posi-
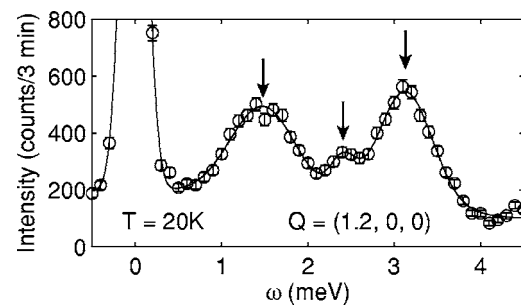
FIG. 4. High-energy-resolution inelastic neutron-scattering scan taken at SPINS at $T=20$ K, with constant $\mathbf{Q}=(1.2,0,0)$ and a fixed final energy of 5 meV. This scan shows three crystal-field modes at 1.48(2), 2.41(3), and 3.13(2) meV indicated by the arrows. The scans at other Q positions reveal that these modes are dispersionless, and polarized beam measurements taken on BT2 (not shown) confirm that they are magnetic.
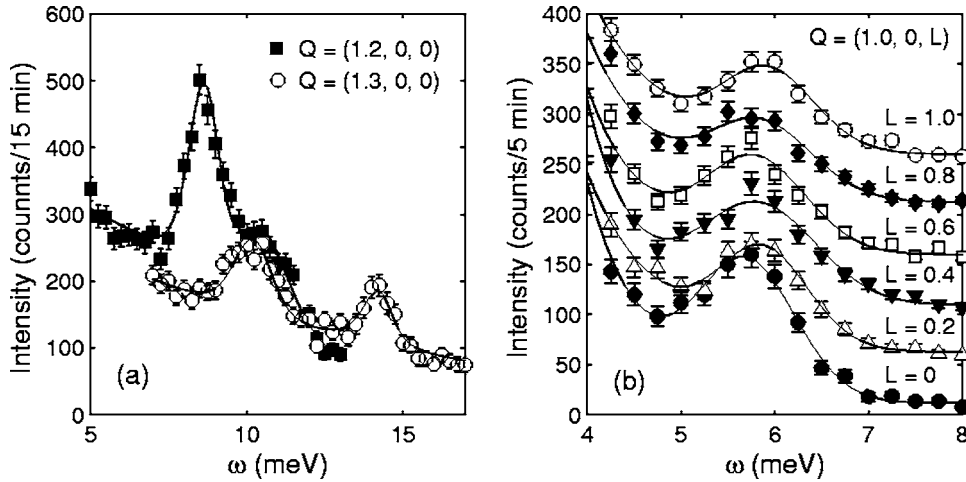
FIG. 5. Typical inelastic neutron-scattering measurements of the spin-wave spectrum. (a) Measurements at different in-plane momentum transfers show two distinct branches with different dispersions. (b) Measurements as a function of out-of-plane momentum transfer shows no dispersion within the errors. The increasing intensity below 5 meV is due to the tail end of the 3.13 meV crystal-field level. The location of these inelastic magnetic peaks is used to establish the spin-wave dispersion in Fig. 6.

tions of these excitations obtained from fits of individual scans at 20 K are plotted as circles in Figs. 6(b) and 6(c).

C. Spin-wave calculations

The experimental spin-wave dispersion data were compared to a theoretical model using linear spin-wave analysis. The model assumes a Hamiltonian of the form

$$H = J \sum_{\langle i,j \rangle} \mathbf{S}_i \cdot \mathbf{S}_j + D \sum_i S_i^z S_i^z, \quad (1)$$

where $\langle i,j \rangle$ indicates that the sum is over nearest-neighbor in-plane pairs, J is the primary antiferromagnetic exchange,

and D is the anisotropy. This Hamiltonian is linearized using the Holstein-Primakoff transformation and then mapped onto a quantum harmonic oscillator, similarly to Ref. 21. The lattice Fourier sum is defined as

$$z = \frac{1}{12} \{ e^{-2\pi i (H/3 - K/3)} + e^{2\pi i (2H/3 + K/3)} + e^{-2\pi i (H/3 + 2K/3)} \}. \quad (2)$$

Because of the noncollinear spin structure, the spin-wave dispersion has three modes with corresponding lattice Fourier sums:

$$z_1 = z + z^*,$$

$$z_2 = -(z + z^*)/2 + i(\sqrt{3}/2)(z - z^*),$$

$$z_3 = -(z + z^*)/2 - i(\sqrt{3}/2)(z - z^*). \quad (3)$$

The dispersion relationship is then given by

$$\omega_i = 3SJ\sqrt{(1 + 4z_i + 2D/3J)(1 - 2z_i)}, \quad (4)$$

where $i = 1$, 2, or 3, and $S = 2$ is the spin of the Mn^{3+} ion. The three modes are equivalent but offset from each other, with the zeros of each mode (where $\omega_i = 0$) occuring at different positions in reciprocal space, as shown in Fig. 6(a).

The 20 K experimental data in Figs. 6(b) and 6(c) were fitted to Eq. (4) using J and D as fitting parameters. The lines show results of the fit, with $J = 2.44(8)$ meV and $D = 0.38$. J determines the overall scaling of the dispersion curve, while D is responsible for the zone-center gap around 5.5 meV. Fits of data at 50 K show little change in J, but did show a significant decrease in D.[19] In order to establish the temperature dependence of D, the zone-center gap was measured at several additional temperatures and used to determine D assuming a fixed J, and the results are plotted in Fig. 7. D shows a continuous decrease with increasing temperature, but no abrupt change in the region around T_{SR}.

FIG. 6. (a) The $(H,K,0)$ plane of the reciprocal lattice for HoMnO₃. The black circles indicate the zeros of mode 1, open triangles the zeros of mode 2, and gray squares the zeros of mode 3. The dashed lines indicate magnetic zone boundaries. [(b) and (c)] Spin-wave dispersion along the high-symmetry directions [indicated by the vertical and horizontal arrows, respectively, in (a)]. The circles indicate neutron data taken at 20 K, lines indicate fits of the data to the three modes of the dispersion curve given by Eq. (4), with $J = 2.44(7)$ meV and $D = 0.38(8)$ meV.

III. DISCUSSION

At higher temperatures the H-T phase diagram obtained from neutron scattering agrees well with previous dielectric[9] and SHG (Ref. 15) measurements, though the reported transition temperatures vary somewhat. At low temperatures, the comparison becomes problematic. Neutron scattering reveals
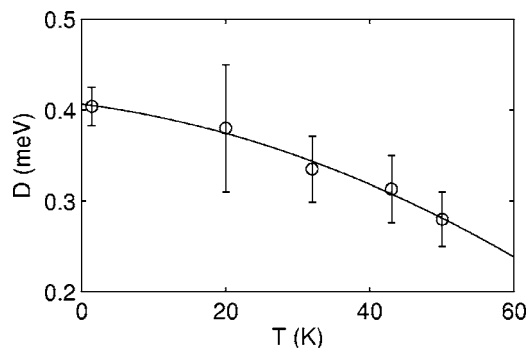
FIG. 7. The single-ion anisotropy D as a function of temperature. The value at 20 K is obtained from fitting data to Eq. (4) using J and D as fitting parameters. Data at other temperatures are obtained using $J=2.44$ meV fixed. The line shows a quadratic fit to the data.

two unambiguous and distinct intermediate phases.[19] In contrast, magnetic susceptibility and heat capacity measurements show only a single intermediate phase below 3 K, which spans approximately the same range in field as the combined intermediate phases oberved by neutrons.[20] More recent measurements of the dielectric constant reveal similar complexity at low temperatures, including apparent intermediate transitions with hysteresis, but still only reveal a single intermediate phase below 3 K.[10]

It is not yet clear whether this difference is due to differences in the experimental probe or in the samples themselves. Sample differences are the likely cause of discrepancies in zero-field transition temperatures, with $T_{SR}=33$ K reported from dielectric constant and magnetometry work[9,20] compared with $T_{SR} \approx 40$ K for the samples used in the current neutron-scattering work. Such sample variations (possibly due to residual stresses, nonstoichiometric oxygen, or impurity contamination) cannot be ruled out yet as causes for the differences in the observed phase diagram from these different techniques. Furthermore, although the identification of observed phase boundaries from neutron scattering is unambiguous, the actual structure of these intermediate phases has not yet been determined. In order to determine the structure in these phases, measurements of out-of-plane peaks are needed, which will require the use of a horizontal-field magnet.

In contrast to the phase diagram, the spin dynamics of $HoMnO_3$ measured by neutrons has so far proven to be much easier to interpret. Despite the simplicity of the magnetic Hamiltonian, the agreement between theory and experiment is excellent. Additional terms in the Hamiltonian are clearly necessary in order to produce the complex phase diagram observed experimentally, but the strength of any additional terms should be much weaker than the established values for J and D. Within experimental limits, J is constant as a function of temperature, but D has a clear temperature dependence. The continuous variation of D suggests that this may simply follow the evolution of the lattice constants, where a decreases and c increases with decreasing temperature in the ordered phase. There are anomalies in the expansivity at T_{SR},[18] but these anomalies are small enough that the change in lattice constants is close to continuous across T_{SR}.

The 2D nature of the spin dynamics is easily understood in terms of the structure of $HoMnO_3$, where the in-plane separation of Mn ions is much smaller than the out-of-plane separation. Furthermore, because of the offset in stacking between adjacent Mn layers, the out-of-plane interactions should be almost completely frustrated. Ferroelectric lattice distortions may relieve the interplane frustration in $HoMnO_3$,[3] and may be the driving force behind the spin reorientation transitions of the Mn magnetic lattice. Ho may play a role in these transitions similar to the role of Nd in Nd_2CuO_4, another layered transition-metal oxide with weak, frustrated interplanar interactions. Nd_2CuO_4 has a noncollinear structure,[22] and the rare-earth single-ion anisotropy of the Nd ions drives several spin reorientation transitions as a function of temperature.[23,24]

Finally, these results can be compared with neutron-scattering measurements on $YMnO_3$, which has a structure very close to $HoMnO_3$, though with a much simpler phase diagram with no zero-field spin reorientation transitions. The magnetic Hamiltonian proposed for $YMnO_3$ (Ref. 25) is actually more complicated than the model proposed here for $HoMnO_3$. The largest terms in the Hamiltonian for $YMnO_3$ ($J_1=3.4$ meV, $J_2=2.02$ meV, and $D=0.28$ meV) are similar to the values obtained for $HoMnO_3$ ($J=2.44$ meV and a temperature-dependent D around 0.4 meV at low temperature, decreasing at higher temperatures). The prominent crystal-field excitations in $HoMnO_3$, absent from the scattering data for $YMnO_3$, make measurements of the low-energy spin-wave spectrum more complicated. Without additional information on the low-energy region of the spin-wave spectrum, the additional terms in the Hamiltonian for $YMnO_3$ such as interplane coupling cannot be included in the description of $HoMnO_3$. Measurements of the low-energy spin wave spectrum are currently in progress, and preliminary results suggest that the spin waves interact with the crystal-field levels. These interactions may play an important role in the spin reorientation transitions in $HoMnO_3$ and may explain why the phase diagram of $HoMnO_3$ is so much more complex than $YMnO_3$, which does not exhibit similar crystal-field excitations, despite the similarity in both structure and even in the higher-energy spin-wave spectrum for both materials.

ACKNOWLEDGMENTS

[1] T. Kimura, T. Goto, M. Shintani, K. Ishizaka, T. Arima, and Y. Tokura, Nature (London) **426**, 55 (2003).
[2] N. Hur, S. Park, P. A. Sharma, J. S. Ahn, S. Guha, and S. Cheong, Nature (London) **429**, 392 (2004).
[3] T. Lottermoser, T. Lonkai, U. Amann, D. Hohlwein, J. Ihringer, and M. Fiebig, Nature (London) **430**, 541 (2004).
[4] N. A. Hill, J. Phys. Chem. B **104**, 6694 (2000).
[5] H. L. Yakel, W. C. Koehler, E. F. Bertaut, and E. F. Forrat, Acta Crystallogr. **16**, 957 (1963).
[6] W. C. Koehler, H. L. Yakel, E. O. Wollan, and J. W. Cable, Phys. Lett. **9**, 93 (1964).

[7]Z. J. Huang, Y. Cao, Y. Y. Sun, Y. Y. Xue, and C. W. Chu, Phys. Rev. B **56**, 2623 (1997).

[8]N. Fujimura, T. Ishida, T. Yoshimura, and T. Ito, Appl. Phys. Lett. **69**, 1011 (1996).

[9]B. Lorenz, A. P. Litvinchuk, M. M. Gospodinov, and C. W. Chu, Phys. Rev. Lett. **92**, 087204 (2004).

[10]F. Yen, C. R. dela Cruz, B. Lorenz, Y. Y. Sun, Y. Q. Wang, M. M. Gospodinov, and C. W. Chu, Phys. Rev. B **71**, 180407 (2005).

[11]A. Muñoz, J. A. Alonso, M. J. Martínez-Lope, M. T. Casáis, J. L. Martínez, and M. T. Fernández-Díaz, Chem. Mater. **13**, 1497 (2001).

[12]T. Lonkai, D. Hohlwein, J. Ihringer, and W. Prandl, Appl. Phys. A: Mater. Sci. Process. **74**, S843 (2002).

[13]M. Fiebig, D. Fröhlich, K. Kohn, S. Leute, T. Lottermoser, V. V. Pavlov, and R. V. Pisarev, Phys. Rev. Lett. **84**, 5620 (2000).

[14]M. Fiebig, D. Fröhlich, T. Lottermoser, and K. Kohn, Appl. Phys. Lett. **77**, 4401 (2000).

[15]M. Fiebig, C. Degenhardt, and R. V. Pisarev, J. Appl. Phys. **91**, 8867 (2002).

[16]M. Fiebig, D. Fröhlich, T. Lottermoser, and M. Maat, Phys. Rev. B **66**, 144102 (2002).

[17]H. Sugie, N. Iwata, and K. Kohn, J. Phys. Soc. Jpn. **71**, 1558 (2002).

[18]C. dela Cruz, F. Yen, B. Lorenz, Y. Q. Wang, Y. Y. Sun, M. M. Gospodinov, and C. W. Chu, Phys. Rev. B **71**, 060407(R) (2005).

[19]O. P. Vajk, M. Kenzelmann, J. W. Lynn, S. B. Kim, and S. W. Cheong, Phys. Rev. Lett. **94**, 087601 (2005).

[20]B. Lorenz, F. Yen, M. M. Gospodinov, and C. W. Chu, Phys. Rev. B **71**, 014438 (2005).

[21]A. B. Harris, C. Kallin, and A. J. Berlinsky, Phys. Rev. B **45**, 2899 (1992).

[22]S. Skanthakumar, J. W. Lynn, J. L. Peng, and Z. Y. Li, Phys. Rev. B **47**, R6173 (1993).

[23]R. Sachidanandam, T. Yildirim, A. B. Harris, A. Aharony, and O. Entin-Wohlman, Phys. Rev. B **56**, 260 (1997).

[24]D. Petitgrand, S. V. Maleyev, P. Bourges, and A. S. Ivanov, Phys. Rev. B **59**, 1079 (1999).

[25]T. J. Sato, S. Lee, T. Katsufuji, M. Masaki, S. Park, J. R. D. Copley, and H. Takagi, Phys. Rev. B **68**, 014432 (2003).